NATIONAL ADVISORY COMMITTEE FOR AERONAUTICS

TECHNICAL NOTE 3122

EXPERIMENTAL INVESTIGATION AT A MACH NUMBER OF 2.41 OF AVERAGE SKIN-FRICTION COEFFICIENTS AND VELOCITY PROFILES FOR LAMINAR AND TURBULENT BOUNDARY LAYERS AND AN ASSESSMENT OF PROBE EFFECTS

By Robert M. O'Donnell

Langley Aeronautical Laboratory
Langley Field, Va.

Washington
January 1954

NATIONAL ADVISORY COMMITTEE FOR AERONAUTICS

TECHNICAL NOTE 3122

EXPERIMENTAL INVESTIGATION AT A MACH NUMBER OF 2.41 OF AVERAGE SKIN-FRICTION COEFFICIENTS AND VELOCITY PROFILES FOR LAMINAR AND TURBULENT BOUNDARY LAYERS AND AN ASSESSMENT OF PROBE EFFECTS

By Robert M. O'Donnell

SUMMARY

An experimental investigation was made of laminar and turbulent boundary layers on the outer surface of a hollow cylinder at a Mach number of 2.41 and over a Reynolds number range of 0.06×10^6 to 0.95×10^6 per inch. Boundary-layer surveys were made by means of a total-pressure probe for stations ranging from 0.58 to 8.08 inches from the leading edge.

In the absence of probe effects, the experimental results for the laminar boundary layer showed good agreement with the laminar theory of Chapman and Rubesin, while those for the turbulent boundary layer showed good agreement with the extended Frankl and Voishel analysis of Rubesin, Maydew, and Varga. The experimental turbulent velocity profiles were found to agree closely with a 1/7-power profile; the constant of the 1/7-power profile derived experimentally showed excellent agreement with the empirical constant of Cope and Watson. With no probe interference, transition Reynolds numbers increased with increasing tunnel stagnation pressure.

The experimentally determined value of the constant in the equation predicting the rate of growth of the laminar boundary layer along the model agreed well with the theoretical value. The finite size of probe used in the investigation measured laminar skin-friction coefficients as predicted by theory. This probe had a width-height ratio of 4.8 and gave satisfactory results provided the ratio of probe height to boundary-layer thickness was no greater than 0.22. Where probe interference was significant, the effect of the probe was either to cause early transition of the laminer boundary layer or to distort the velocity profiles so that abnormally high average skin-friction coefficients were measured.

INTRODUCTION

Recent experimental investigations (refs. 1 to 4) of average skin-friction coefficients for laminar boundary layers, involving total-pressure surveys through the boundary layer on a flat plate, have produced average skin-friction coefficients that are considerably higher than those predicted by theory. Reference 5 reports an investigation of the effects of Reynolds number and boundary-layer development along the surfaces of hollow cylinders having their axes parallel to the free-stream flow direction. It was concluded that the leading-edge thickness had a pronounced effect on the development of the boundary layer and that the size of the probe may have had some effect on measurements near the leading edge of the model. The experimental results also indicated that results essentially the same as those for a flat plate could be obtained from boundary-layer surveys on a hollow cylinder. In an effort to determine the cause of the discrepancy between experimental flat-plate results and laminar-boundary-layer theory, a detailed investigation, reported in reference 6, was made of the effects of probe size, heat transfer through the leading-edge region, leading-edge geometry, and strength of the leading-edge shock wave. Of all these effects, only the probe effect was found to be significant, and the conclusion was reached that only a probe of vanishing height would measure the theoretically predicted values.

The purpose of this report is to present the results of an investigation on a hollow cylinder, at a Mach number of 2.41, of the effects of Reynolds number and a total-pressure probe on the local and average skin-friction coefficients for laminar boundary layers, and the effect of Reynolds number on local and average skin-friction coefficients for turbulent boundary layers that are formed as a result of natural transition.

SYMBOLS

b	constant in 1/7-power velocity profile
c_f	local skin-friction coefficient
C_f	average skin-friction coefficient
G	constant in equation for boundary-layer growth
h	outside height of probe tip, in.
l	distance along model from leading edge to calculated origin of turbulent flow, in.

M	Mach number
N	constant in formula defining momentum thickness of turbulent boundary layer
p	local static pressure, in. Hg abs
p_o	stagnation pressure, in. Hg abs
r	outside radius of model, in.
R_x	Reynolds number based on distance from leading edge, $\rho_1 U_1 x/\mu_1$
R_Θ	Reynolds number based on three-dimensional momentum thickness, $\rho_1 U_1 \Theta/\mu_1$
R_{x_T}	Reynolds number of transition, $\rho_1 U_1 x_T/\mu_1$
u	velocity within boundary layer, ft/sec
U	velocity, ft/sec
x	distance along model from leading edge, in.
y	distance normal to model, in.
γ	ratio of specific heat at constant pressure to specific heat at constant volume (1.40 for air)
δ	boundary-layer thickness at 99 percent of free-stream Mach number, in.
θ	two-dimensional momentum thickness of boundary layer, in.
Θ	three-dimensional momentum thickness of boundary layer on a cylindrical body, in.
μ	coefficient of viscosity, slugs/ft-sec
ρ	density, slugs/cu ft

Subscripts:

1	conditions at outer edge of boundary layer
T	conditions at transition

APPARATUS

Wind Tunnel

All tests were conducted in the Langley 9-inch supersonic tunnel, which is a continuous-operation, closed-circuit type in which the pressure, temperature, and humidity of the enclosed air can be regulated. Different test Mach numbers are provided by interchangeable nozzle blocks which form test sections approximately 9 inches square. Eleven fine-mesh turbulence-damping screens are installed ahead of the supersonic nozzle in a settling chamber of relatively large area. A schlieren optical system is provided for qualitative flow observations.

Hollow Cylinder

The hollow steel cylinder used in the tests is shown schematically in figure 1(a). The model, which is $1\frac{7}{8}$ inches in diameter and 22 inches long, was turned, ground, and polished to a surface roughness of approximately 5 root-mean-square microinches. The leading edge of the cylinder was chamfered to an angle of 5° and rounded to a thickness of about 0.0020 inch to avoid feathering.

Static-pressure orifices were located on the top, bottom, and sides of the model. Nine orifices were provided on the survey side, beginning 1/2 inch from the leading edge and spaced 1 inch apart for a total distance of $8\frac{1}{2}$ inches. The circumferential position of this row of orifices was approximately 0.21 inch from the line of survey. Two orifices placed on each of the other three sides were spaced 4 inches apart, the first one being located $2\frac{1}{2}$ inches from the leading edge.

The hollow cylinder was mounted from the side wall of the tunnel as shown in figure 1(c).

Boundary-Layer Survey Apparatus

The apparatus used to support the total-pressure probe is shown in figures 1(b) and 1(c). The exterior mechanism operates in the same way as a standard micrometer and is graduated in thousandths of an inch. In order to obtain rigidity, the supporting mechanism inside the tunnel was composed of two double-wedge struts with the smaller one sliding inside the larger (see fig. 2(a)). The assembled apparatus is mounted on a circular metal plate that replaces one of the tunnel windows.

The total-pressure probe was constructed according to the procedure given in reference 7, of 0.020-inch stainless-steel tubing that was flattened and stoned to the dimensions shown in figure 2(b). Contact of the probe with the cylinder surface was indicated by a low-amperage electrical contact system.

PROCEDURE

Tests were conducted at a free-stream Mach number of 2.41 within a Reynolds number range of approximately 0.06×10^6 to 0.95×10^6 per inch. This Reynolds number range was obtained by varying the tunnel stagnation pressure from about 7 to 120 in. Hg abs with a corresponding stagnation-temperature range of 93° to 125° F. The dew point of the tunnel was kept sufficiently low so as to insure negligible condensation effects.

Static-pressure measurements on the model surface were obtained at stagnation pressures of 7, 30, 60, 90, and 120 in. Hg abs, with schlieren observations being made at each of these pressures.

Total-pressure measurements were made through the boundary layer at eight stations. These survey stations were located along the center line of the model, the first and last stations being 0.58 inch and 8.08 inches, respectively, from the model leading edge. Distance of the probe from the model surface was measured by means of the micrometer attachment (fig. 1(b)); probe position could be measured within ±0.00025 inch and repeated within approximately ±0.00050 inch. The surveys were made at stagnation pressures of 7, 30, 60, 90, and 120 in. Hg abs for each station. Static, impact, and tunnel stagnation pressures were measured on a mercury manometer. The impact-pressure probe had a response time of approximately 20 seconds; however, in order to minimize the chances of error, a minute was allowed for the impact-pressure reading to settle out.

REDUCTION OF PRESSURE-SURVEY DATA

By making the conventional assumptions that within the boundary layer the static pressure and total temperature are constant normal to the model surface, the velocity profile may be calculated from the Mach number survey for the case of zero heat transfer by means of the expression

$$\frac{u}{u_1} = \frac{M}{M_1}\sqrt{\frac{1 + \frac{\gamma - 1}{2} M_1^2}{1 + \frac{\gamma - 1}{2} M^2}} \tag{1}$$

Two-dimensional momentum thickness is defined as

$$\theta = \int_0^{\delta} \frac{\rho u}{\rho_1 u_1}\left(1 - \frac{u}{u_1}\right) dy \tag{2}$$

where

$$\frac{\rho}{\rho_1} = \frac{1 + \frac{\gamma - 1}{2} M^2}{1 + \frac{\gamma - 1}{2} M_1^2} \tag{3}$$

By the proper substitution of the expressions for density and velocity ratio, the expression for two-dimensional momentum thickness may be obtained in terms of Mach number and y only.

In this investigation, some correction to the momentum-thickness expression must be made to account for the cylindrical form of the model. The method used in reference 5 was also used in the present investigation. The expression for three-dimensional momentum thickness, when put into terms of Mach number and y, is then given by

$$\Theta = \theta + \frac{1}{rM_1^2}\int_0^{\delta} \left(MM_1 \sqrt{\frac{1 + \frac{\gamma - 1}{2} M^2}{1 + \frac{\gamma - 1}{2} M_1^2}} - M^2 \right) y \, dy \tag{4}$$

where the second term is the correction for form.

This form correction amounted to a maximum of about 4 percent for the position farthest downstream. No corrections were made to the momentum thickness to account for small variations of Mach number along the model surface.

PRECISION OF DATA

Static, impact, and tunnel stagnation pressures are accurate to an estimated ±0.01 in. Hg. This value results in a Mach number error of ±0.06 at the lowest stagnation pressure and ±0.005 at the highest. The Reynolds number error of the investigation is approximately ±4,000 per inch.

On the basis of the given accuracy in Mach number and of the probe positioning mechanism, the error in the determination of momentum thickness is estimated to be no greater than 1 percent, and the accuracy in the determination of local skin-friction coefficients from the faired plots of momentum thickness is about 10 percent.

RESULTS AND DISCUSSION

Static-Pressure Distribution

The longitudinal static-pressure distribution on the cylinder is presented in figure 3 for various stagnation pressures. Measurements of static pressure on the top, bottom, and sides of the model show little variation, the greatest discrepancies being at the lowest stagnation pressure of 7 in. Hg abs. These results indicate that the Mach number distribution on the model is relatively constant, and hence the assumption of a zero pressure gradient appears to be justified.

Schlieren Observations

A typical schlieren photograph of the flow over the cylinder is given in figure 4 for a stagnation pressure of 60 in. Hg abs. Natural transition is assumed to occur at the point on the model where the boundary layer suddenly starts to thicken (indicated by the arrow in the figure). It can be seen that a disturbance from the nozzle blocks is present on the top side of the tunnel test section. This disturbance intersects only a small portion of the model near the leading edge and is known to be relatively weak from past surveys of the stream; the weakness of the disturbance is indicated indirectly in figure 4 by the fact that it closely parallels the disturbance from the model leading edge, whose strength is little more than that of a Mach wave. The exact effect of this tunnel disturbance upon transition on this model is not known, but it is evidently small since, as is shown subsequently, extensive laminar runs are obtained and the Reynolds number for transition is of the proper magnitude as compared with unpublished results. In any case, the effect has no bearing on the assessment of probe interference since it is always present.

Velocity Profiles

Nondimensional velocity profiles are shown in figures 5 to 9 for stagnation pressures of 7, 30, 60, 90, and 120 in. Hg abs. It can be seen in figure 5, which represents the lowest stagnation pressure, that the experimental laminar velocity profiles agree well with the laminar-boundary-layer theory of Chapman and Rubesin (ref. 8).

In figure 6 are shown laminar, transitional, and turbulent velocity profiles. The turbulent profiles are compared with a 1/7-power law with the constant b of the following equation equal to 0.683:

$$\frac{u}{U_1} = b\left(\frac{y}{\theta}\right)^{1/7}$$

The value 0.683 was obtained by systematically varying the value of b until good agreement was obtained between the experimental turbulent velocity profiles and the 1/7-power profile. This estimated value of b shows excellent agreement with the value of 0.685 derived from the results of reference 9. At this pressure the experimental laminar velocity profiles differ slightly from those predicted by theory, while the turbulent velocity profile shows fair agreement with the 1/7-power law. The velocity profile at $x = 6.58$ inches falls between the laminar and turbulent profiles and is therefore considered to be transitional.

At a stagnation pressure of 60 in. Hg abs (fig. 7), the experimental laminar velocity profiles are again different from those predicted by theory, while the turbulent velocity profiles show good agreement with the 1/7-power profile. The velocity profile at $x = 6.58$ inches, which appeared transitional at 30 in. Hg abs, is now completely turbulent, and the velocity profile at 4.58 inches is now evidently transitional. The form and position of the velocity profile at $x = 0.58$ inch indicates that it, too, is transitional. This, however, cannot be the result of natural transition since the velocity profiles occurring at 1.58, 2.58, and 3.58 inches from the leading edge at the same stagnation pressure lie close to the laminar profile.

At stagnation pressures of 90 and 120 in. Hg abs (figs. 8 and 9) some velocity profiles are completely turbulent and good agreement is obtained with the 1/7-power law, whereas others appear transitional. It should be noted that velocity profiles which are obtained near the leading edge at high stagnation pressures and which appear to be turbulent or transitional are not necessarily a result of natural transition but may well be attributed to the disturbance caused by the total-pressure probe in the thinner laminar boundary layer.

Boundary-Layer Transition

It is known that transition points obtained from schlieren photographs as indicated in figure 4 can be correlated with those obtained from total-pressure surveys of the boundary layer. (See ref. 5, for example.) In the present investigation, two methods of obtaining transition points from boundary-layer surveys are presented. The first method assumes transition points to occur at the intersections of the experimental laminar and turbulent curves of figure 10. (Also shown in fig. 10 are the theoretical laminar curves from ref. 8.) However, in this figure the experimental laminar points fall above the theoretical curves at the higher stagnation pressures, so that erroneous transition points result. Approximate locations of the true transition points may be determined by this method when there is probe interference by assuming that the points occur at the intersections of the theoretical turbulent (ref. 10) and theoretical laminar curves. The transition curve determined by this method is presented in figure 11 and is seen to follow the trend of the schlieren results.

In order to determine accurately the limit of probe interference, transition points were determined by a second method. This method also uses the data of figure 10 but is more sensitive to changes in momentum thickness. Transition points determined by this method correspond to the minimum momentum thickness occurring at a given survey station as the Reynolds number is varied by varying tunnel stagnation pressure. Figure 11 shows that this method agrees well with the first method up to a stagnation pressure of about 50 in. Hg abs, after which it diverges rapidly. The latter portion of the curve, however, does not represent the true transition occurring on the model but only the apparent transition as manifested by the probe and is used only in evaluating the limit of probe interference. Figure 12 presents the corresponding Reynolds numbers for transition and shows them increasing with increasing tunnel stagnation pressure when there is no probe interference. (This trend has also been noted in ref. 5.) The two values shown in each of figures 11 and 12 for the schlieren results at p_o = 90 in. Hg abs correspond to the beginning and end of a turbulence burst observed in the schlieren photograph at this pressure. The survey method would not be expected to agree exactly with the schlieren results when there is no probe interference, since the transition points obtained by the survey method were determined from measurements on the side and the schlieren results from measurements on the top of the model. Irregular transition around a model has been discussed in reference 11.

Determination of Effective Leading Edge for Turbulent Flow

The values of momentum thickness presented in figure 10 were used in the calculation of average skin-friction coefficients for both laminar and turbulent flows. However, before these values could be used in the case of turbulent flow, some correction was necessary to account for the fact that the turbulent boundary layer did not start at the leading edge of the model. An effective leading edge was determined by a method similar to that used in reference 4. In this reference it is shown that the variation of momentum thickness with the fifth root of the Reynolds number may be applied to compressible flow; therefore the variation of momentum thickness with Reynolds number and distance from the effective leading edge is given by the formula

$$\theta = \frac{N(x - l)}{(R_{x-l})^{1/5}} \tag{5}$$

where l is the distance from the actual leading edge of the model to the effective leading edge. This distance is shown schematically in the following sketch:

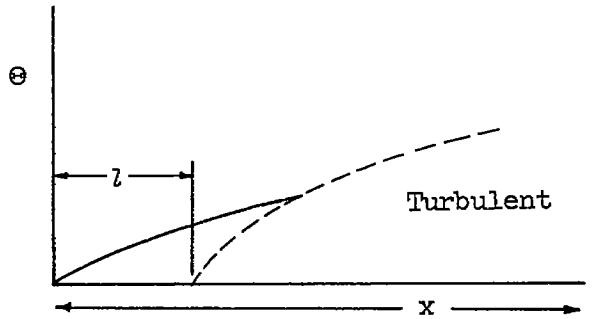

The solution of the equation requires the determination of l, N, and, of course, R_{x-l}. The formula was solved for each stagnation pressure by a trial-and-error procedure; first a value was assigned to l and then the constant N was calculated by using the known experimental values of momentum thickness and a Reynolds number based on $x - l$. The values of l and N were varied systematically until the values of θ calculated from equation (5) agreed closely with the experimental values of θ throughout the turbulent range. These values are given in the following table for momentum-thickness values corresponding to 100 percent turbulent flow:

p_o	l	N
30	5.8	0.0260
60	3.7	.0254
90	2.6	.0261
120	2.0	.0265

(Because of insufficient data at a stagnation pressure of 30 in. Hg abs, the value of the constant N was taken as the average of the three values of N at the higher stagnation pressures, since there is little change in N with p_o.) It can be seen from figure 10 that the experimental points at $x = 6.58$ inches for 30 in. Hg abs and $x = 4.58$ inches for 60 in. Hg abs lie at the intersections of the curves. These points represent profiles that appear transitional in figures 6 and 7. Hence, no attempt was made to correct them for an effective leading edge.

In figure 13 is shown the variation of Reynolds number based on momentum thickness with Reynolds number based on distance from the leading edge. Also shown is the comparison of the experimental data with the laminar-boundary-layer theories of Blasius and of Chapman and Rubesin (ref. 8) and the turbulent skin-friction theory of Frankl and Voishel as extended by reference 10. Good agreement is obtained between experiment and theory.

It should be noted from this figure that for small values of x at a given R_x the value of R_θ appears to lie in the transition region, whereas for larger values of x at the same R_x the value of R_θ lies in the laminar region. This seemingly early transition was also noted in the velocity profiles obtained at 60 in. Hg abs and is attributed to probe interference. This effect might be expected since the thickness of the laminar boundary layer increases with distance from the leading edge, and any finite disturbance created by a total-pressure probe would have a greater effect where the boundary layer is thinnest; hence the probe effect would be strongest at the most forward stations. This probe effect causes the appearance of rapid premature transition that occurs 0.58 inch from the leading edge of the model (fig. 13). It is not definitely known whether the points falling above the curve for laminar theory at low Reynolds numbers and small distances from the leading edge represent transition velocity profiles. They could be the result of distorted laminar profiles caused by the presence of the probe. The phenomenon also occurs in the results of reference 6 for Reynolds numbers less than 10^6. Whether the probe actually causes premature transition at the higher Reynolds numbers or merely distorts the velocity profiles is also not definitely known. However, from the data presented herein the general appearance is that of transition at the higher Reynolds numbers.

In figure 13 some of the points corresponding to completely turbulent flow ($x > 3.58$ inches) occur at values of R_x that also have points for laminar flow. This result is due to the foreshortened length used in the calculation of R_x for the turbulent values, since turbulent flow does not start at the leading edge of the model.

Skin Friction

Figures 14 and 15 present, respectively, the experimental average skin-friction coefficients as a function of the Reynolds number based on momentum thickness R_θ and the Reynolds number based on length of run R_x. From both figures it is evident that, when probe effects are negligible, the experimental average skin-friction coefficients agree closely with theory for laminar and turbulent flow. Therefore, it is possible to measure average laminar skin-friction coefficients, as predicted by theory, by means of a total-pressure probe of finite size.

Figure 14 illustrates more clearly the probe effects upon transition, since R_θ implies more independence of upstream effects than R_x. Transition Reynolds numbers increase with increasing distance from the leading edge for values of x less than 3.58 inches. Therefore, the probe appears to cause premature transition and hence high average skin-friction coefficients for small values of x. The probe effect then gradually diminishes in strength for larger values of x; consequently, the values of transition Reynolds numbers indicated for the larger values of x would be expected to approach those having no probe effect. This trend is illustrated in figure 16, which is a cross plot of figures 11 and 12.

Figure 17 presents local skin-friction coefficients as a function of momentum-thickness Reynolds number. These local skin-friction coefficients were determined from the slopes of the curves of figure 10; hence, their accuracy is limited by the fairing of the curves. A few of the points obtained at a pressure of 60 in. Hg abs fall far below the theoretical curve. These low points are attributed to probe interference, since the effect of the probe is to increase the momentum-thickness values at the lower values of x. This increase alters the slope of the curve of figure 10 and causes an erroneous local skin-friction coefficient.

It has been assumed in the foregoing comparisons that the results for the cylinder can be compared with flat-plate results. This assumption is based upon the results of an analysis presented in reference 12 of the effects of curvature on the laminar boundary layer in incompressible flow. If the relation for incompressible flow can be applied to compressible flow, the maximum increase of the skin-friction coefficient for the cylinder over that for the flat plate would occur at a stagnation pressure of 7 in. Hg abs. Since this increase would amount to only 2.5 percent, the comparisons are probably justified.

Probe Effect

It has been shown that the probe used in the present investigation accurately measured the average laminar skin-friction coefficients at stagnation pressures up to 30 in. Hg abs and that the probe caused distortion of the thinner laminar boundary layer at higher stagnation pressures. From the data obtained, the largest permissible ratio of probe height to boundary-layer thickness h/δ can be determined. The limiting value of this ratio was determined from the velocity profiles chosen by the minimum-momentum-thickness method previously described. For these profiles, values of δ were calculated by assuming that the edge of the boundary layer occurred at the point where the measured Mach number was 99 percent of the Mach number at the outer edge of the boundary layer.

Figure 18 shows the variation with axial distance x of the ratio h/δ_T for the velocity profiles selected. A discontinuity appears in the experimental curve at about $x = 4.6$ inches. The left leg of this curve ($x < 4.6$ inches) corresponds to those data that are affected by the probe. It therefore appears that the critical value of h/δ_T is roughly 0.23. This value may, however, be more exactly determined by putting the results of figure 18 into a form similar to that used in reference 6. This procedure is as follows. From reference 13 it is known that the laminar boundary-layer thickness in incompressible flow varies according to the relation

$$\delta = \frac{5x}{\sqrt{R_x}} \tag{6}$$

However, in compressible flow the boundary-layer thickness increases with Mach number and the constant in this equation must be determined accordingly. Equation (6) is therefore written

$$\delta = \frac{Gx}{\sqrt{R_x}} \tag{7}$$

where G is the constant dependent on Mach number.

Manipulation of equation (7) yields

$$\frac{h}{x^2} = \frac{h}{\delta}\frac{G}{x\sqrt{R_x}} \tag{8}$$

where the term h/x^2 is the correlation factor of reference 6.

By use of the experimental data of figure 18, values of h/x^2 and $1/x\sqrt{R_x}$ were calculated and are plotted in figure 19. The discontinuity that appears at $x = 4.6$ inches in figure 18 occurs in this figure at $\frac{h}{x^2} \approx 0.00022$. The value of x corresponding to this point is 4.76 inches. The lowest value of h/x^2 obtained from the data of reference 6 was 0.00044 at a Mach number of 3.0. By referring now to figure 18, the critical value of h/δ_T is found to be exactly 0.22. With these results, the value of G is readily determined from equation (8) and is equal to 7.1. A curve obtained by inserting this value of G into equation (7) and dividing each side into h is shown in figure 18 for comparison purposes. A limiting curve for probe interference for the Mach number of this investigation was calculated from equation (8) and is presented in figure 19. All points above the solid line represent interference-free data, whereas points below it are subject to the disturbance caused by the probe. This figure is intended to serve as a guide in deciding whether a probe similar to that used in the present investigation will cause interference in a laminar boundary layer being investigated at a comparable Mach number. Inherent in the interpretation of the figure is the already justified assumption that values of h/δ greater than 0.22 are subject to probe interference.

An examination was made to determine whether the experimental value of G could be reasonably predicted from existing theory. However, in comparing the theoretical constant with the experimental constant, the fact that the Mach number in the test section changes significantly at very low stagnation pressures must be taken into account. At 7 in. Hg abs the average Mach number indicated by the probe was 2.29. From reference 14 the theoretical value of G at a Mach number of 2.29 was found to be 7.27. The value of G at the higher pressures ($M = 2.41$) was found to be about 7.47. It can be seen that within this range of Mach number the change in G is small and the agreement between the theoretical constant and the experimentally determined value of 7.1 is good. Figure 20 presents a comparison between the experimental growth of the boundary layer at a stagnation pressure of 7 in. Hg abs and the prediction of reference 14. Also included is the prediction based on the experimentally determined value of G at transition. The predicted growth is seen to agree closely with experiment.

The preceding results and analyses have been based on the assumption that probe height (in relation to boundary-layer thickness) is the predominant source of probe interference effects, and this assumption appears to be substantiated by existing experimental results, particularly those of reference 6. Nevertheless, comparison of the results of the present investigation with those of reference 6 for a probe having the same height but twice the width indicates that there may be significant effects of

probe width. Comparison of the results of references 6 and 15, however, on a similar basis gives no positive indication of width effect, but the probe installations of these references were somewhat different. At the present time, the experimental data appear to be insufficient to establish a criterion for probe width, but in the present investigation a probe having a width-height ratio of 4.8 gave satisfactory results, provided the ratio of probe height to boundary-layer thickness h/δ was no greater than 0.22.

CONCLUSIONS

Tests were conducted in the Langley 9-inch supersonic tunnel at a free-stream Mach number of 2.41 to investigate the effects of Reynolds number and probe interference on the local and average skin-friction coefficients for laminar boundary layers, and the effect of Reynolds number on the local and average skin-friction coefficients for turbulent boundary layers. The Reynolds number range of the tests was from approximately 0.06×10^6 to 0.95×10^6 per inch for stations ranging from 0.58 to 8.08 inches from the leading edge. The results of this investigation appear to justify the following conclusions:

1. In the absence of probe effects, the experimental results for the laminar boundary layer showed good agreement with the laminar theory of Chapman and Rubesin, while those for the turbulent boundary layer showed good agreement with the extended Frankl and Voishel analysis of Rubesin, Maydew, and Varga when an effective leading edge was established for the turbulent run.

2. With no probe interference, transition Reynolds numbers increased with increasing tunnel stagnation pressure.

3. Experimental turbulent velocity profiles were found to agree closely with a 1/7-power profile, and the constant of the 1/7-power profile derived experimentally showed excellent agreement with the empirical constant of Cope and Watson.

4. The finite size of probe used in the investigation measured laminar skin-friction coefficients as predicted by the theory of Chapman and Rubesin. This probe had a width-height ratio of 4.8 and gave satisfactory results provided the ratio of probe height to boundary-layer thickness was no greater than 0.22.

5. The experimentally determined value of the constant in the equation predicting the rate of growth of the laminar boundary layer along the model agreed well with the theoretical value obtained from the results of NACA TN 2916.

6. For the conditions where probe interference was significant, the probe either caused early transition of the laminar boundary layer or distorted the profiles so that abnormally high average skin-friction coefficients were measured.

Langley Aeronautical Laboratory,
National Advisory Committee for Aeronautics,
Langley Field, Va., October 27, 1953.

REFERENCES

1. Maydew, Randall C., and Pappas, Constantine C.: Experimental Investigation of the Local and Average Skin Friction in the Laminar Boundary Layer on a Flat Plate at a Mach Number of 2.4. NACA TN 2740, 1952.

2. Higgins, Robert W., and Pappas, Constantine C.: An Experimental Investigation of the Effect of Surface Heating on Boundary-Layer Transition on a Flat Plate in Supersonic Flow. NACA TN 2351, 1951.

3. Blue, Robert E.: Interferometer Corrections and Measurements of Laminar Boundary Layers in Supersonic Stream. NACA TN 2110, 1950.

4. Monaghan, R. J., and Johnson, J. E.: The Measurement of Heat Transfer and Skin Friction at Supersonic Speeds. Part II - Boundary Layer Measurements on a Flat Plate at M = 2.5 and Zero Heat Transfer. Tech. Note No. Aero. 2031, Sup. 99, British R.A.E. (Tech. Rep. 13064, A.R.C. C.P. No. 64), Dec. 1949.

5. Brinich, Paul F., and Diaconis, Nick S.: Boundary-Layer Development and Skin Friction at Mach Number 3.05. NACA TN 2742, 1952.

6. Blue, Robert E., and Low, George M.: Factors Affecting Laminar Boundary Layer Measurements in a Supersonic Stream. NACA TN 2891, 1953.

7. Bradfield, W. S., and Yale, G. E.: Small Pitot Tubes With Fast Pressure Response Time. Jour. Aero. Sci. (Reader's Forum), vol. 18, no. 10, Oct. 1951, pp. 697-698.

8. Chapman, Dean R., and Rubesin, Morris W.: Temperature and Velocity Profiles in the Compressible Laminar Boundary Layer With Arbitrary Distribution of Surface Temperature. Jour. Aero. Sci., vol. 16, no. 9, Sept. 1949, pp. 547-565.

9. Cope, W. F., and Watson, G. G.: Preliminary Measurements of the Boundary Layer in the 11-In. Supersonic Wind Tunnel. R. & M. No. 2304, British A.R.C., Aug. 1946.

10. Rubesin, Morris W., Maydew, Randall C., and Varga, Steven A.: An Analytical and Experimental Investigation of the Skin Friction of the Turbulent Boundary Layer on a Flat Plate at Supersonic Speeds. NACA TN 2305, 1951.

11. Potter, J. L.: New Experimental Investigations of Friction Drag and Boundary Layer Transition on Bodies of Revolution at Supersonic Speeds. NAVORD Rep. 2371, U. S. Naval Ord. Lab. (White Oak, Md.), Apr. 24, 1952.

12. Seban, R. A., and Bond, R.: Skin-Friction and Heat-Transfer Characteristics of a Laminar Boundary Layer on a Cylinder in Axial Incompressible Flow. Jour. Aero. Sci., vol. 18, no. 10, Oct. 1951, pp. 671-675.

13. Schlichting, H.: Lecture Series "Boundary Layer Theory." Part I - Laminar Flows. NACA TM 1217, 1949.

14. Klunker, E. B., and McLean, F. Edward: Effect of Thermal Properties on Laminar-Boundary-Layer Characteristics. NACA TN 2916, 1953.

15. Bradfield, W. S., DeCoursin, D. G., and Blumer, C. B.: Characteristics of Laminar and Turbulent Boundary Layer at Supersonic Velocity. Res. Rep. No. 83, Rosemount Aero. Labs., Univ. Minn. Inst. Tech., July 1952.

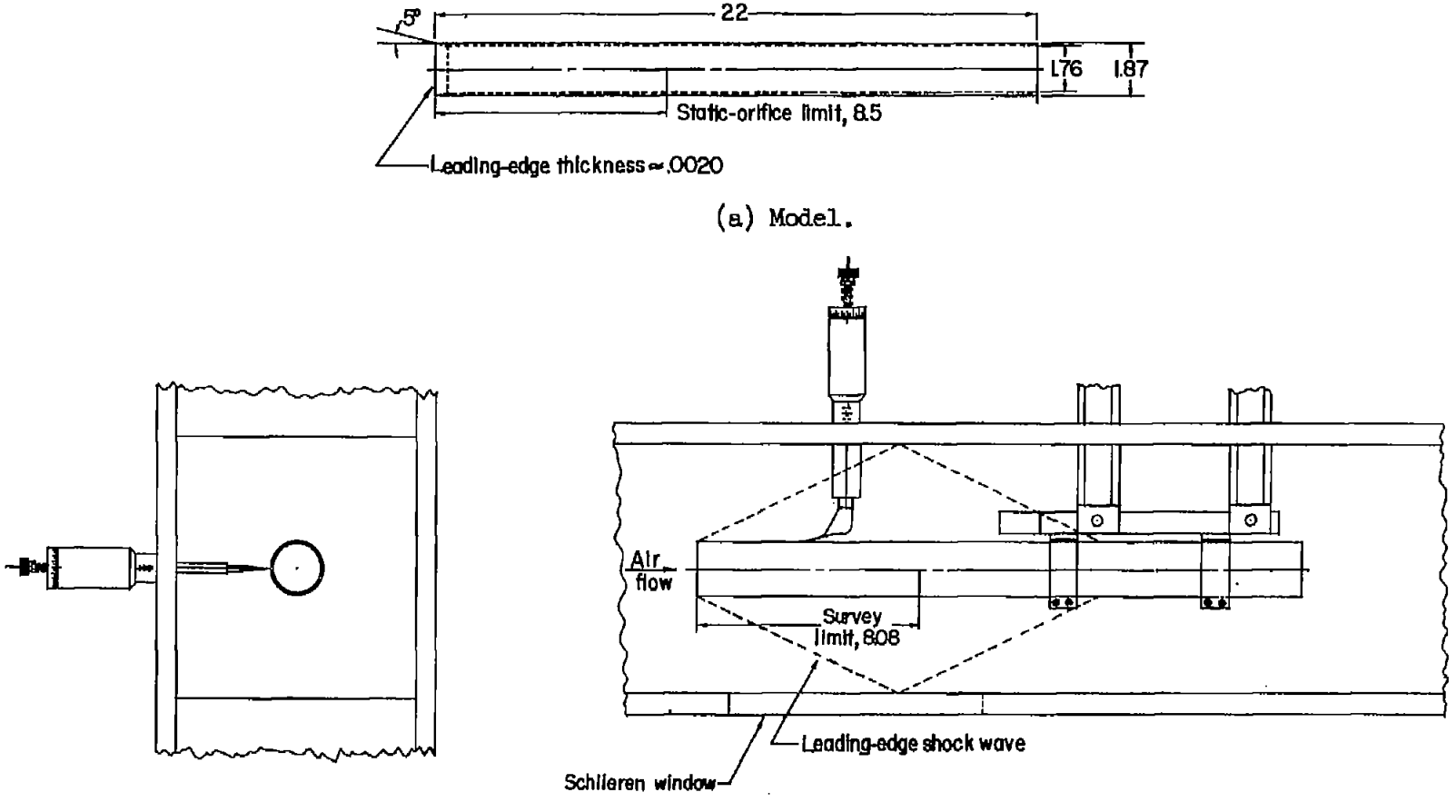

(a) Model.

(b) Front view.

(c) Top view.

Figure 1.- Sketches of hollow cylinder and test installation. All linear dimensions are in inches.

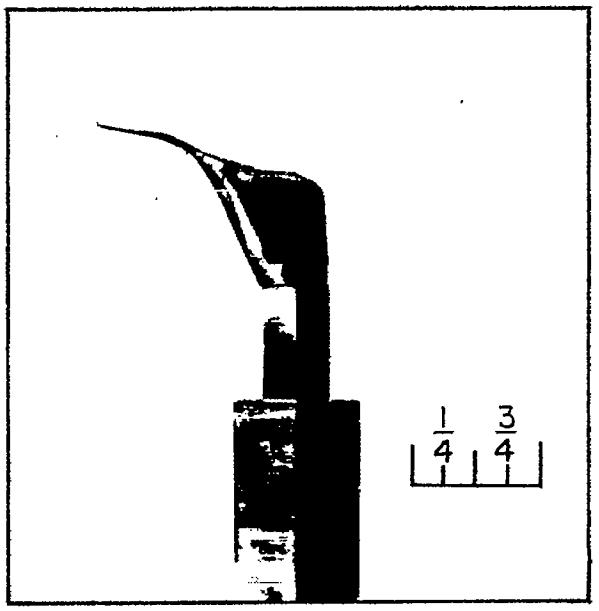

(a) Photograph of probe-supporting mechanism.

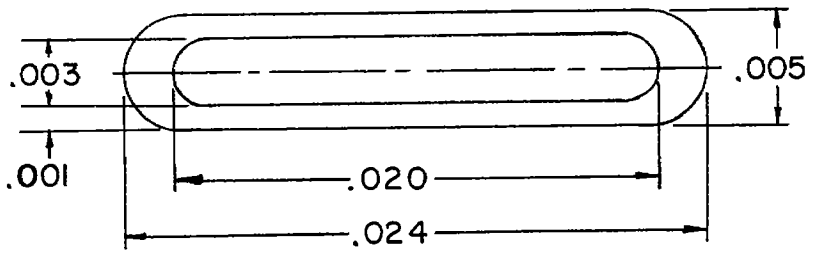

(b) Enlarged view of probe face.

Figure 2.- Total-pressure probe used for boundary-layer survey. All dimensions are in inches.

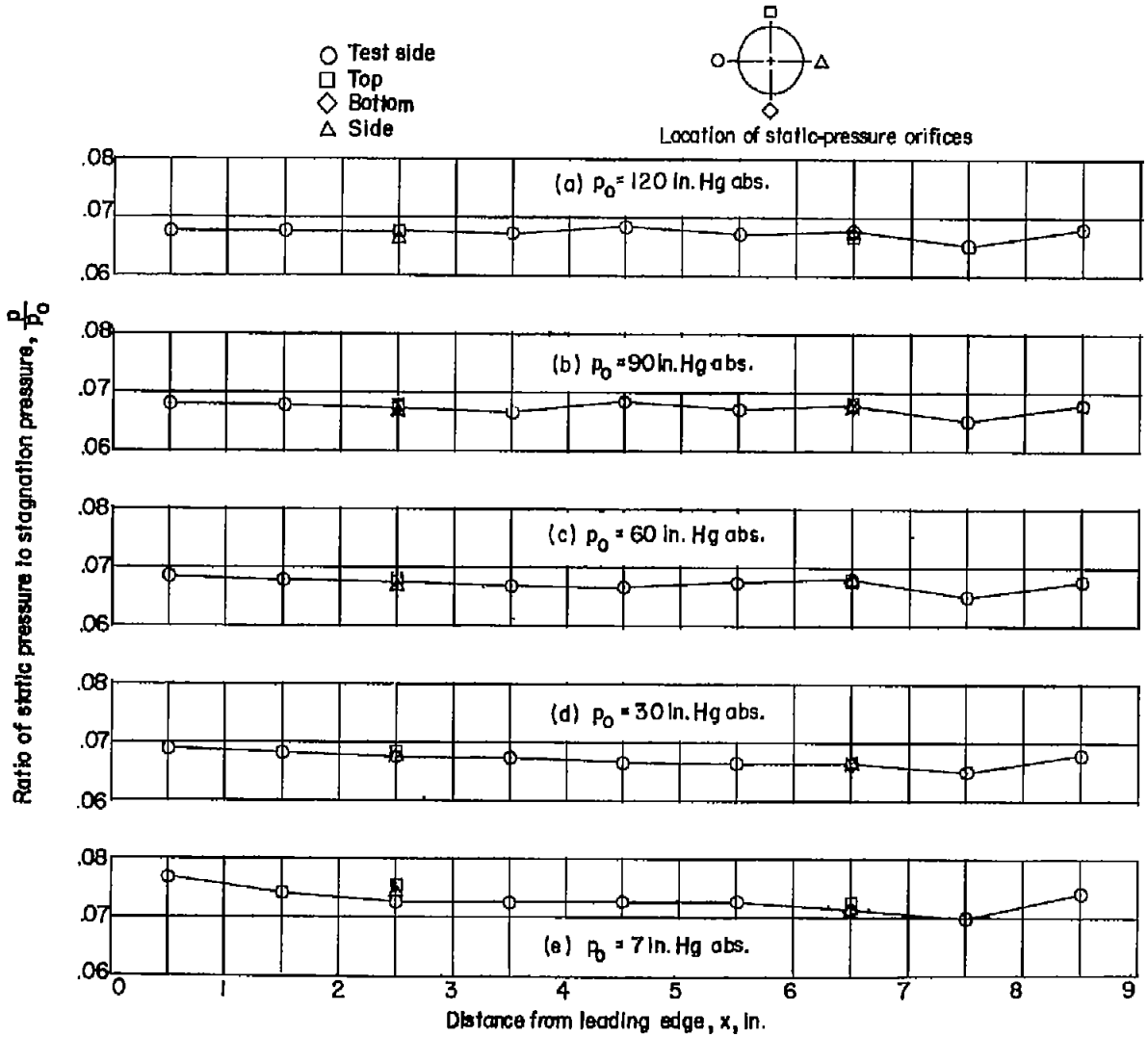

Figure 3.- Static-pressure distribution along the model.

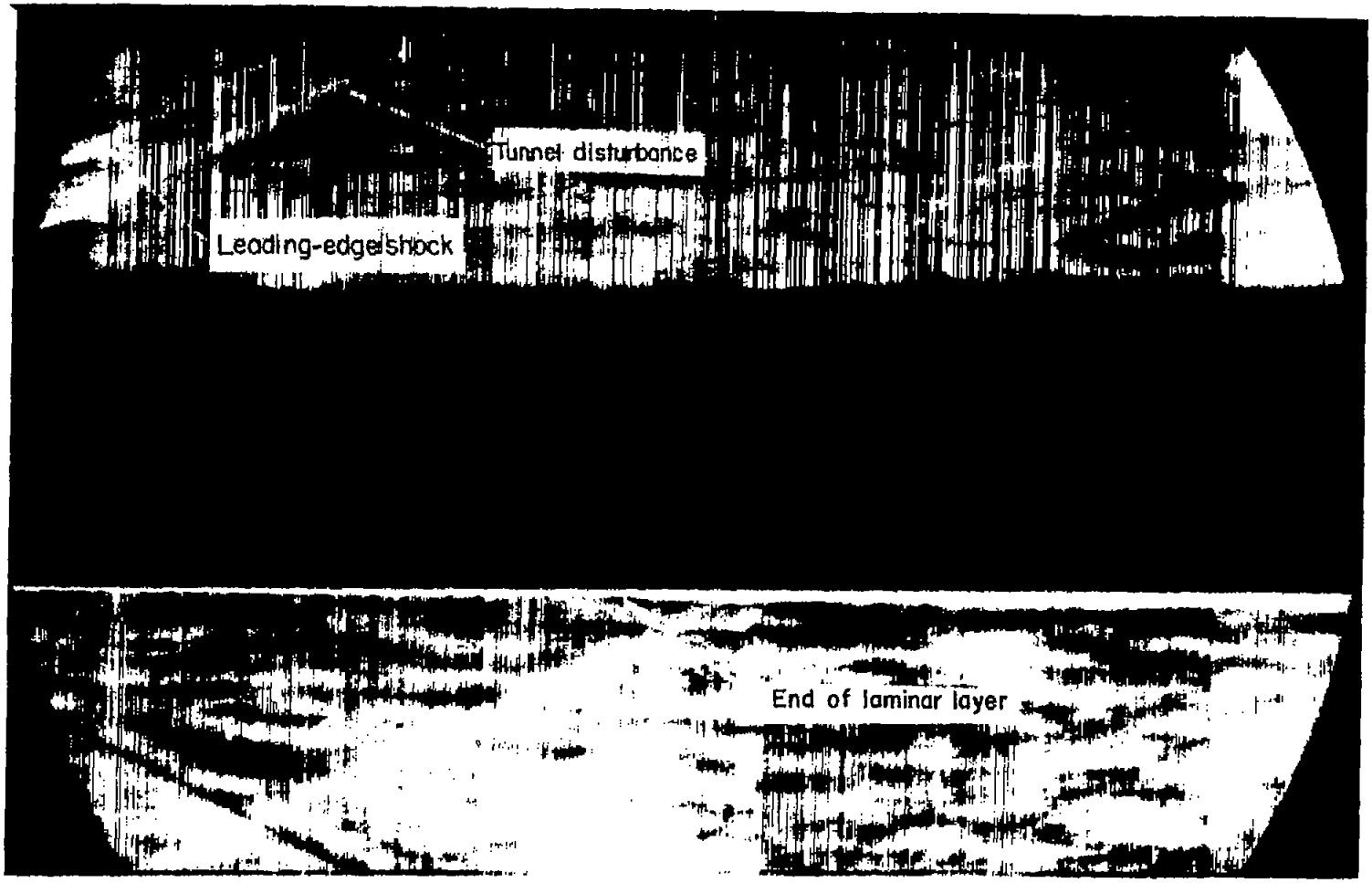

L-81278

Figure 4.- Schlieren photograph of model illustrating natural transition at p_o = 60 in. Hg abs.

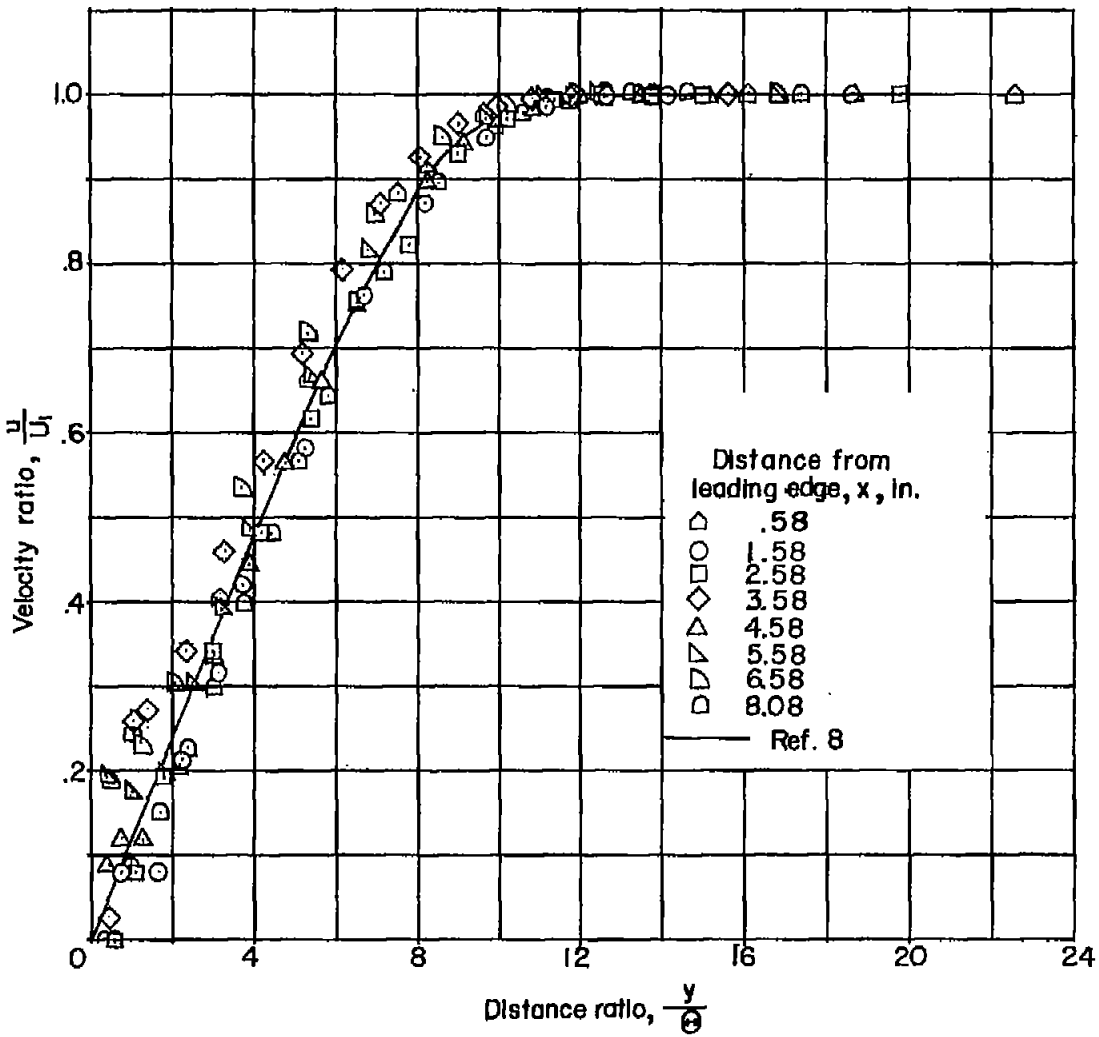

Figure 5.- Laminar velocity profiles compared with theory at p_o = 7 in. Hg abs.

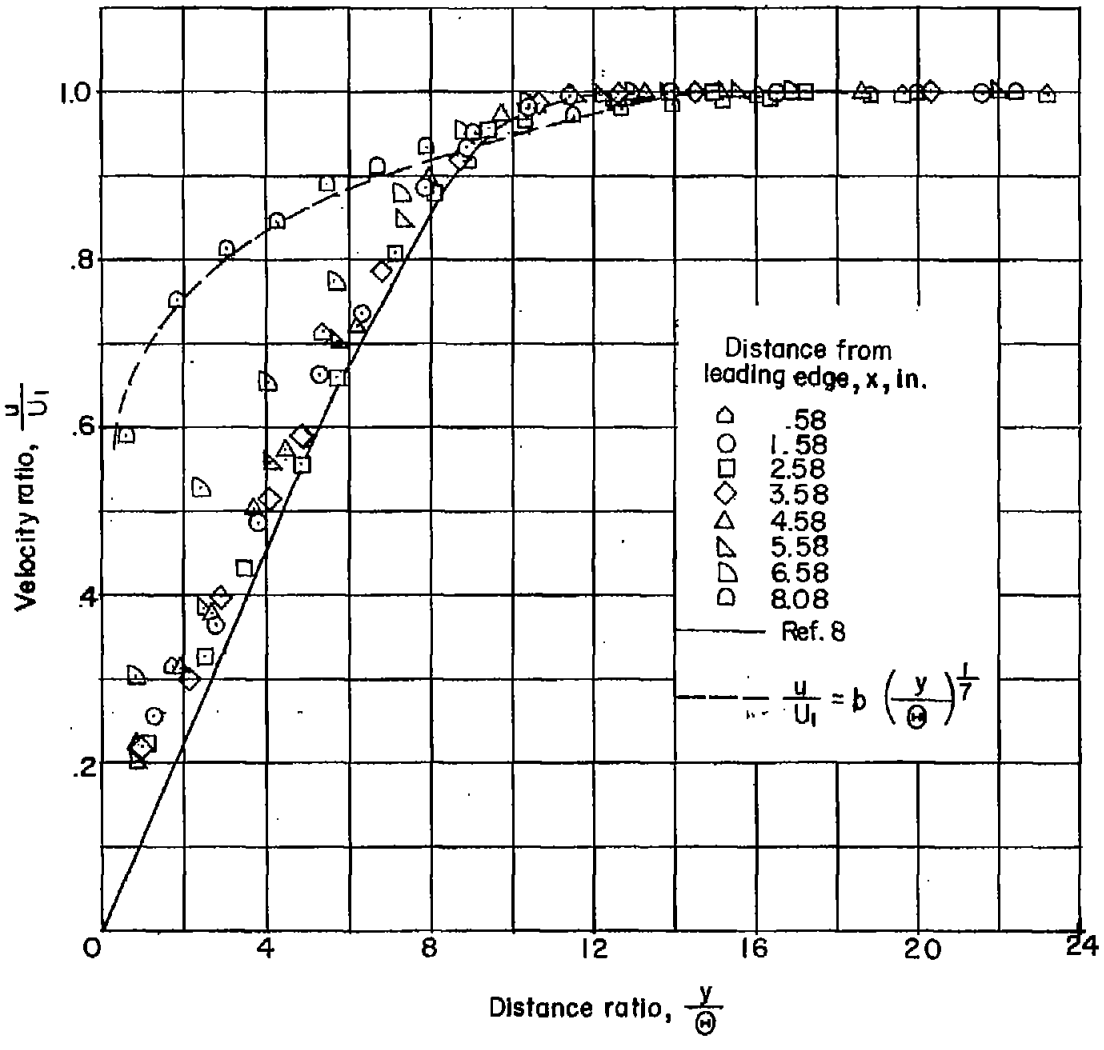

Figure 6.- Laminar and turbulent velocity profiles compared with theory and a 1/7-power profile at p_o = 30 in. Hg abs.

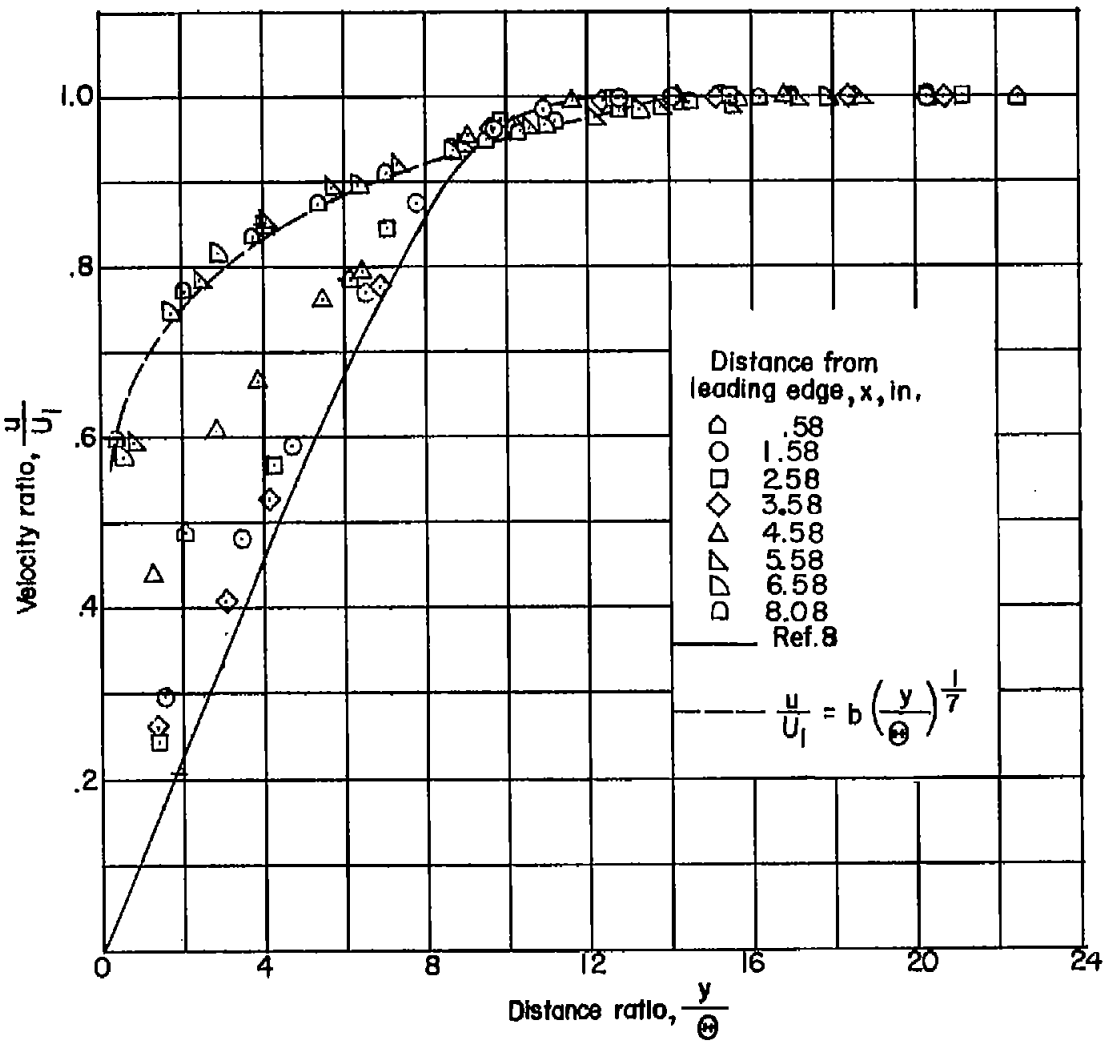

Figure 7.- Laminar and turbulent velocity profiles compared with theory and a 1/7-power profile at p_o = 60 in. Hg abs.

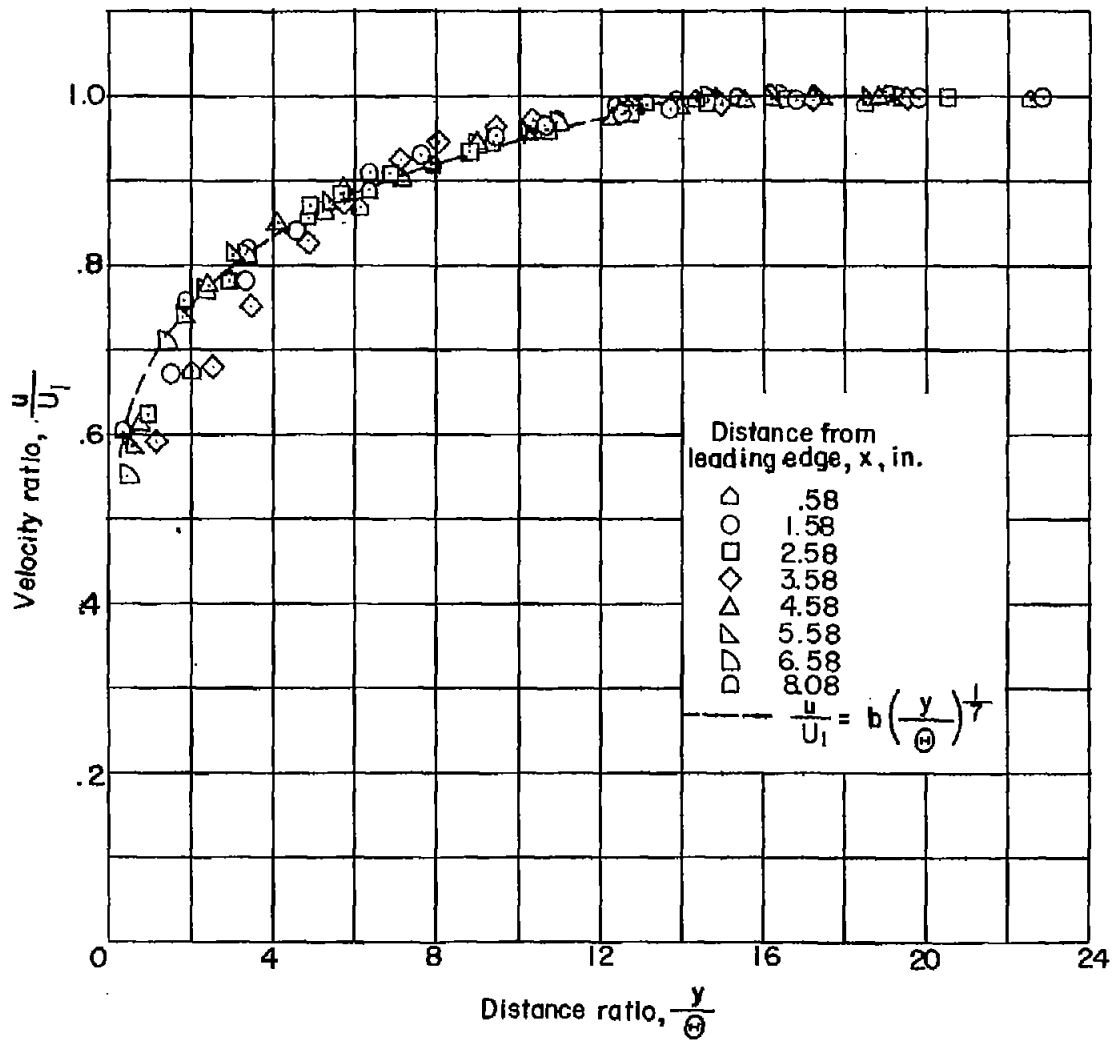

Figure 8.- Turbulent velocity profiles compared with a 1/7-power profile at p_o = 90 in. Hg abs.

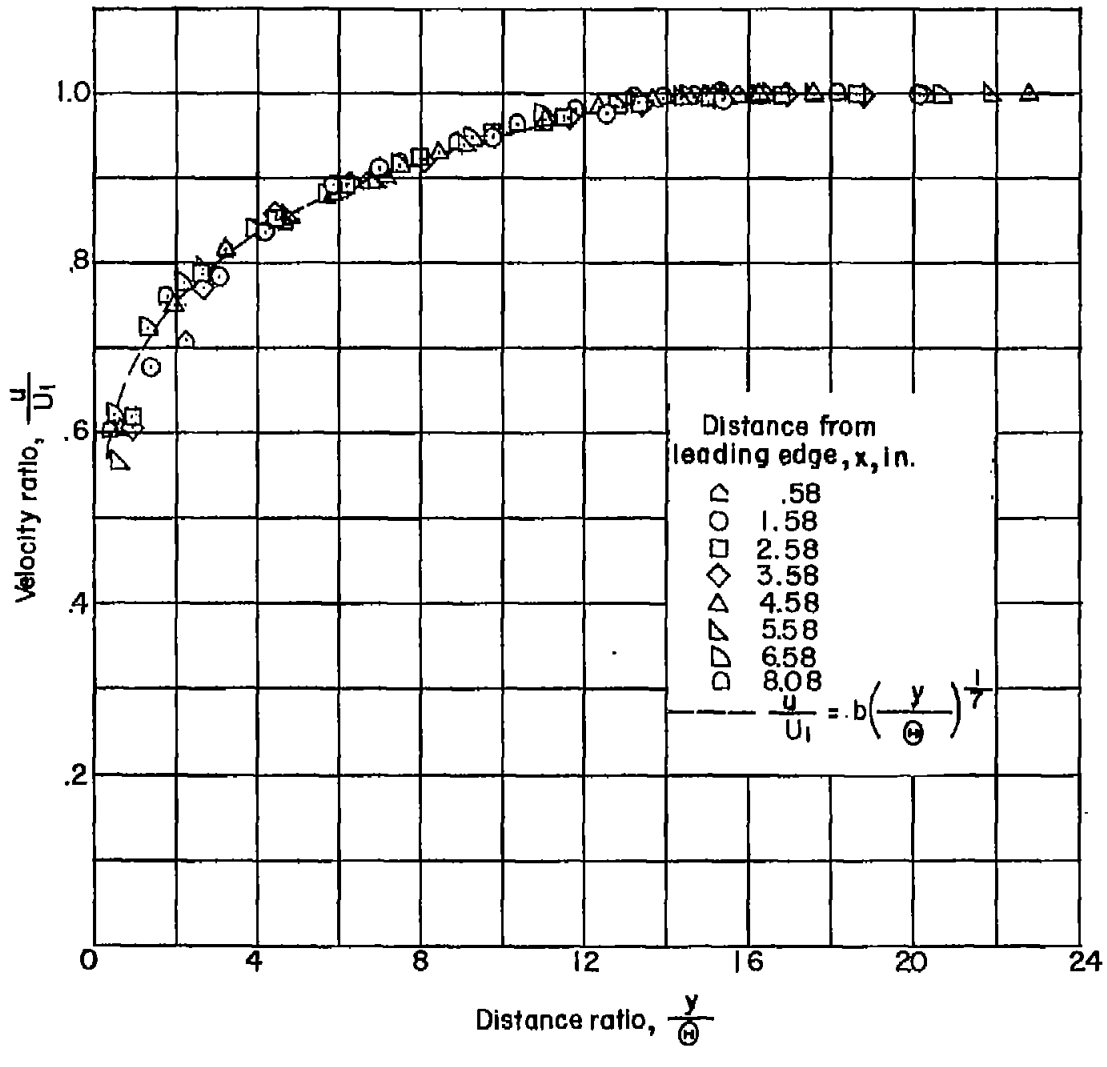

Figure 9.- Turbulent velocity profiles compared with a 1/7-power profile at p_o = 120 in. Hg abs.

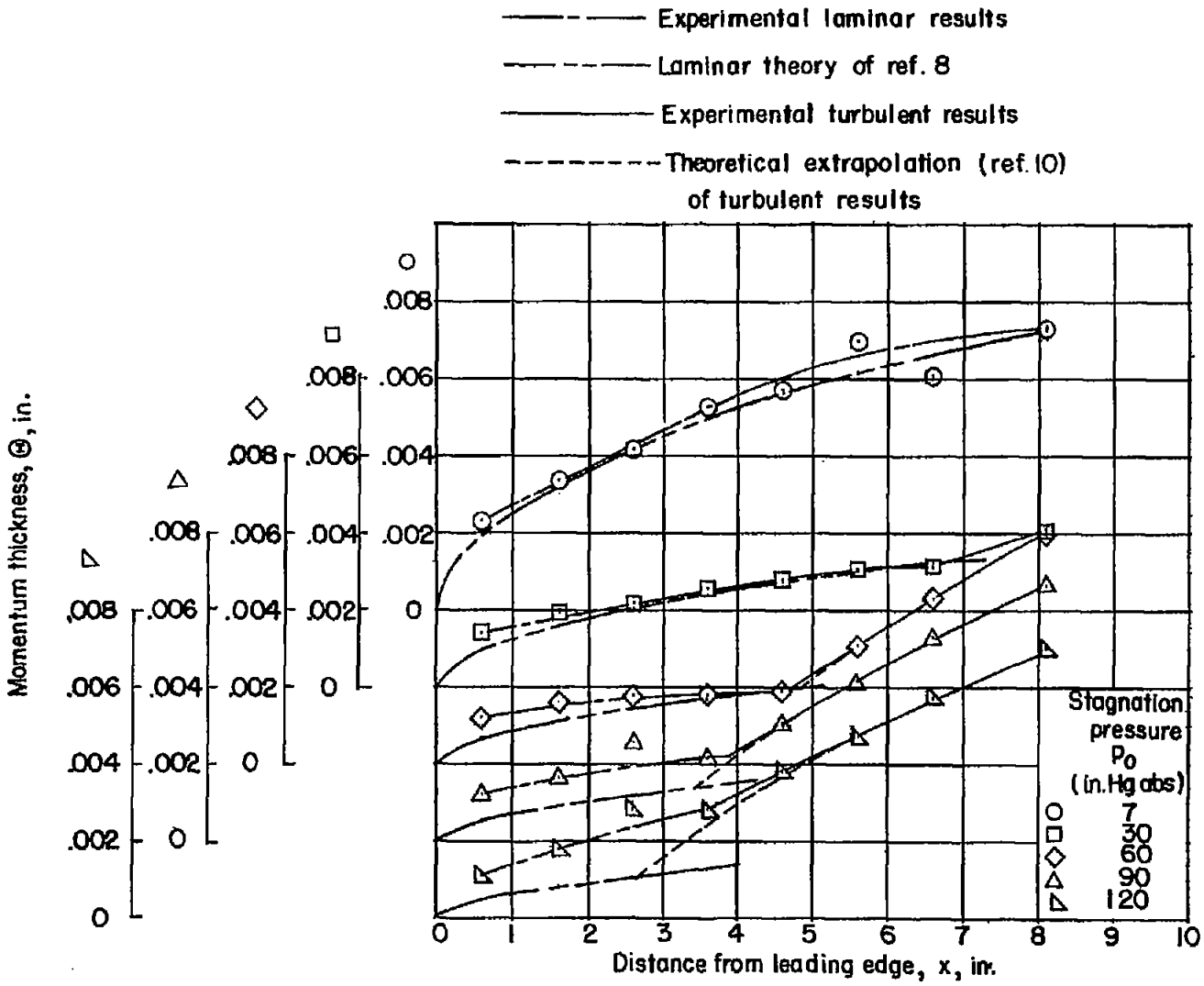

Figure 10.- Momentum-thickness distribution along the model.

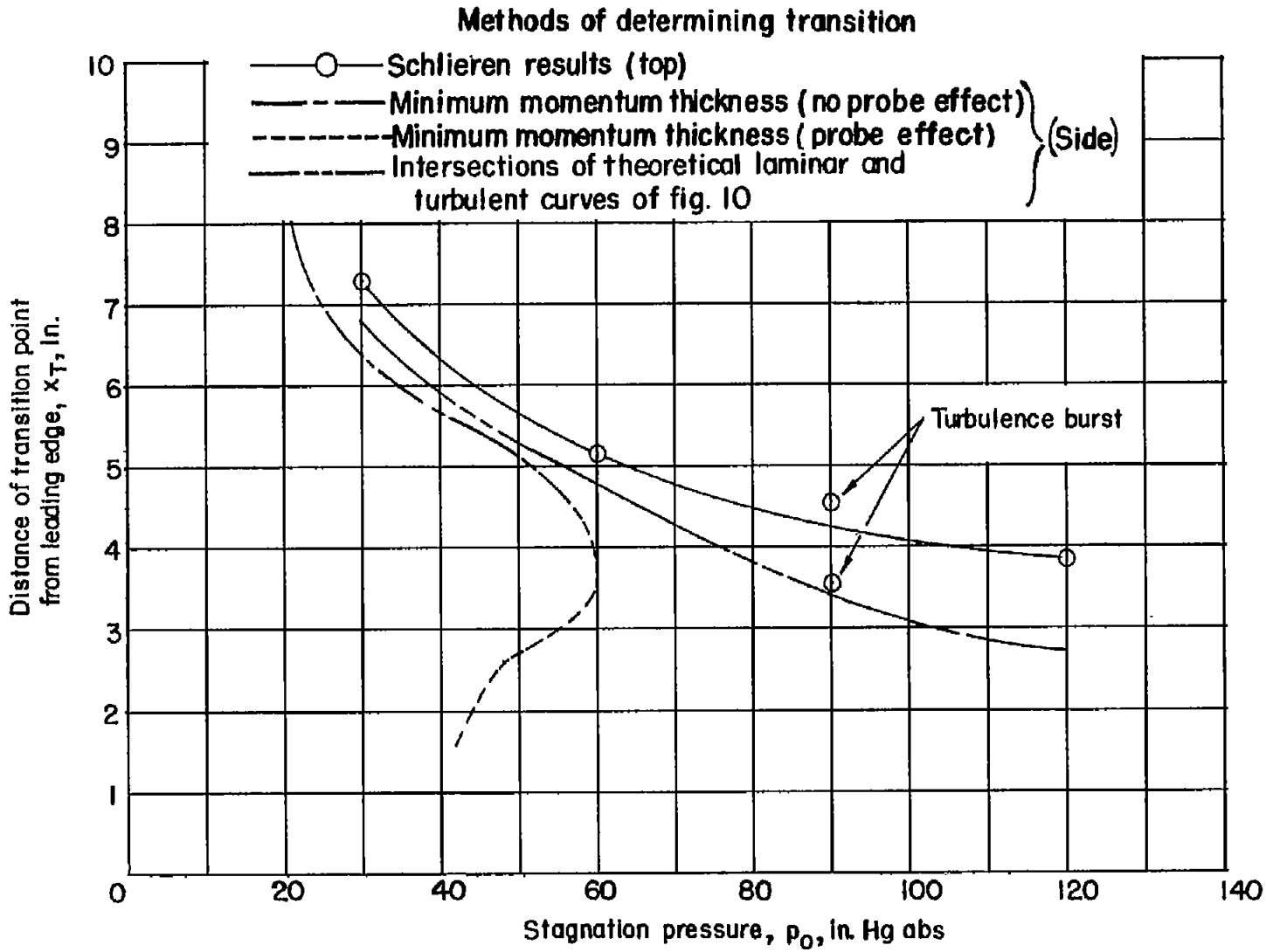

Figure 11.- Variation of transition point with stagnation pressure.

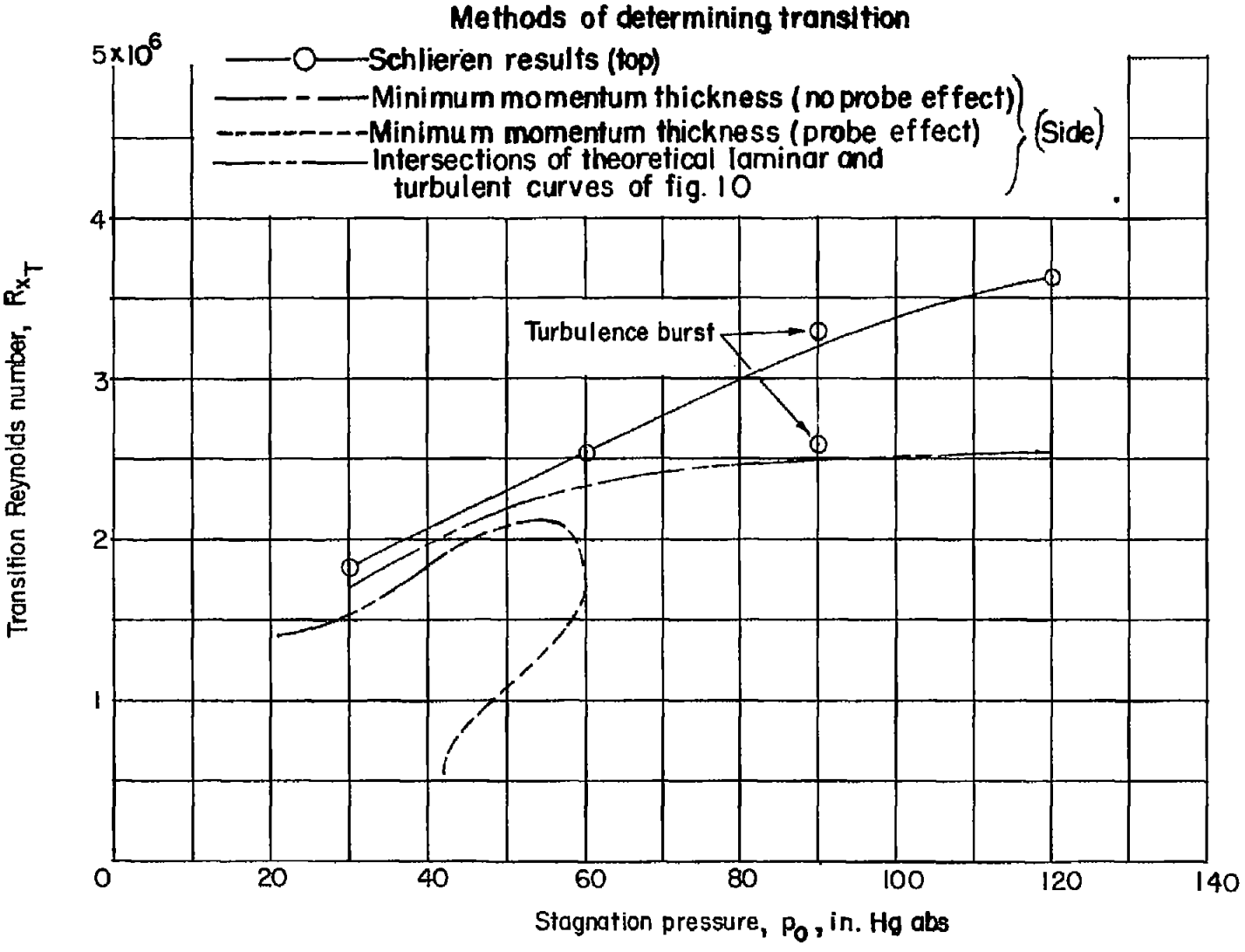

Figure 12.- Variation of transition Reynolds number with stagnation pressure.

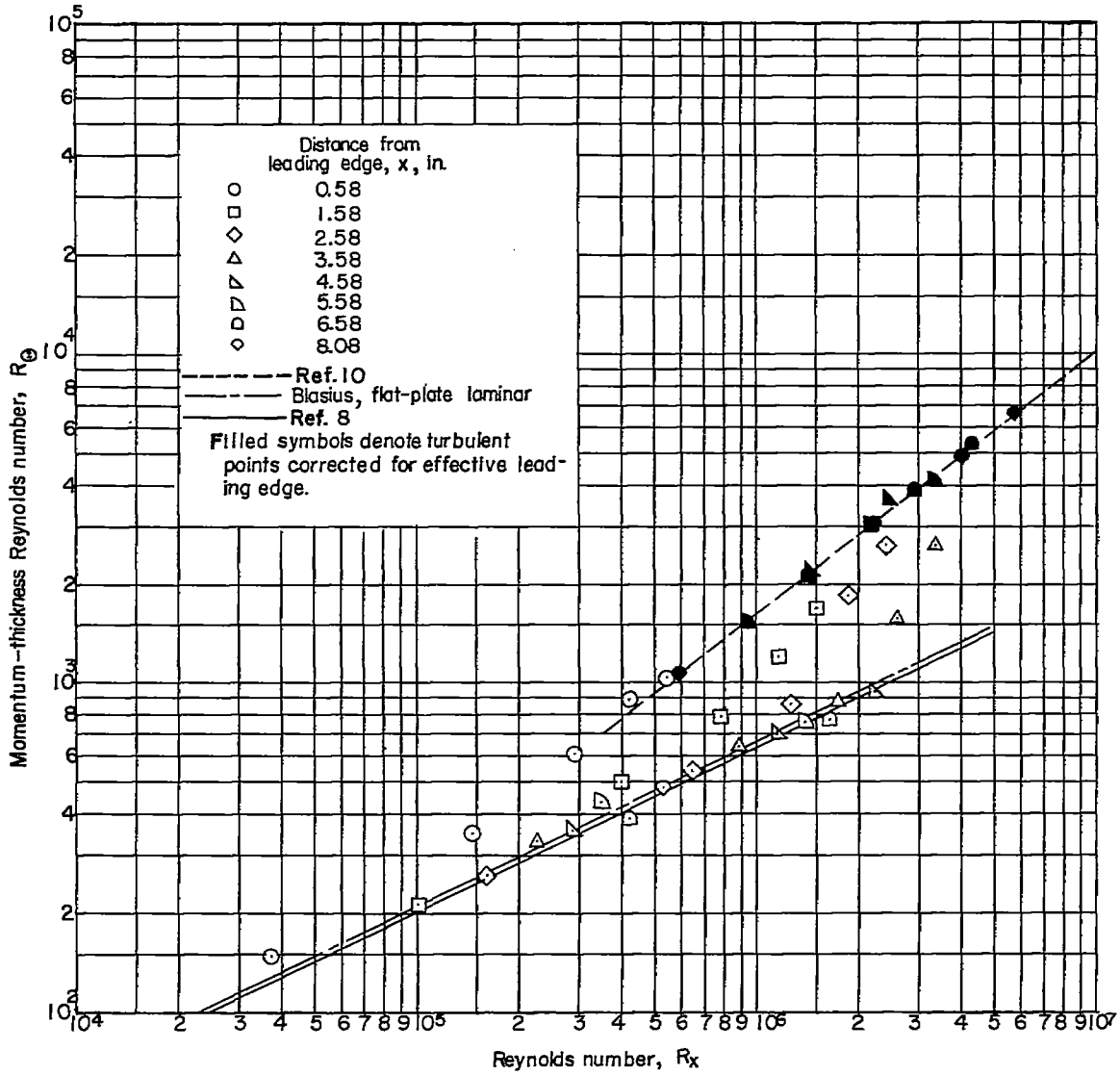

Figure 13.- Variation of momentum-thickness Reynolds number with R_x and comparison with theory.

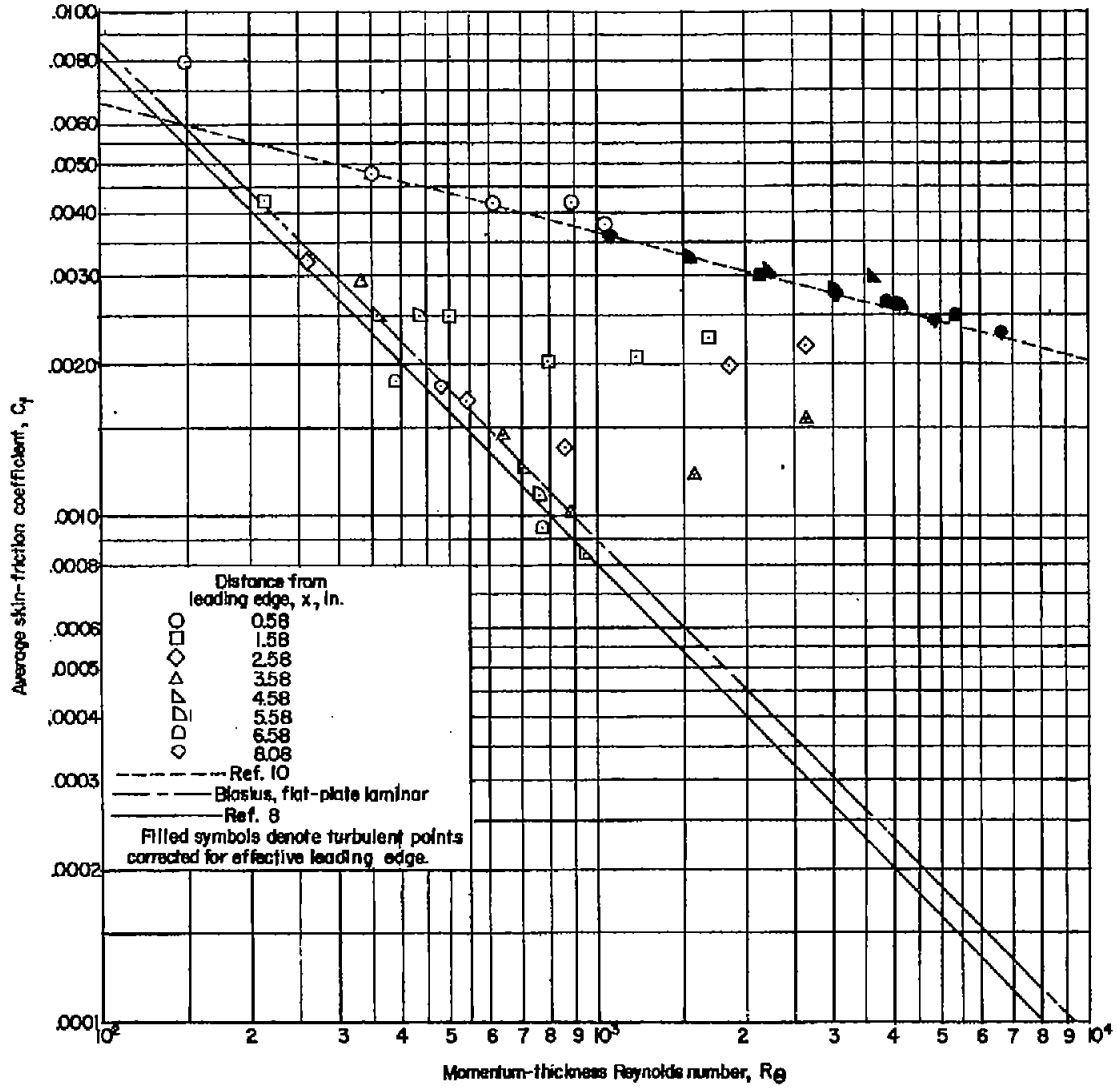

Figure 14.- Variation of average skin-friction coefficient with R_θ.

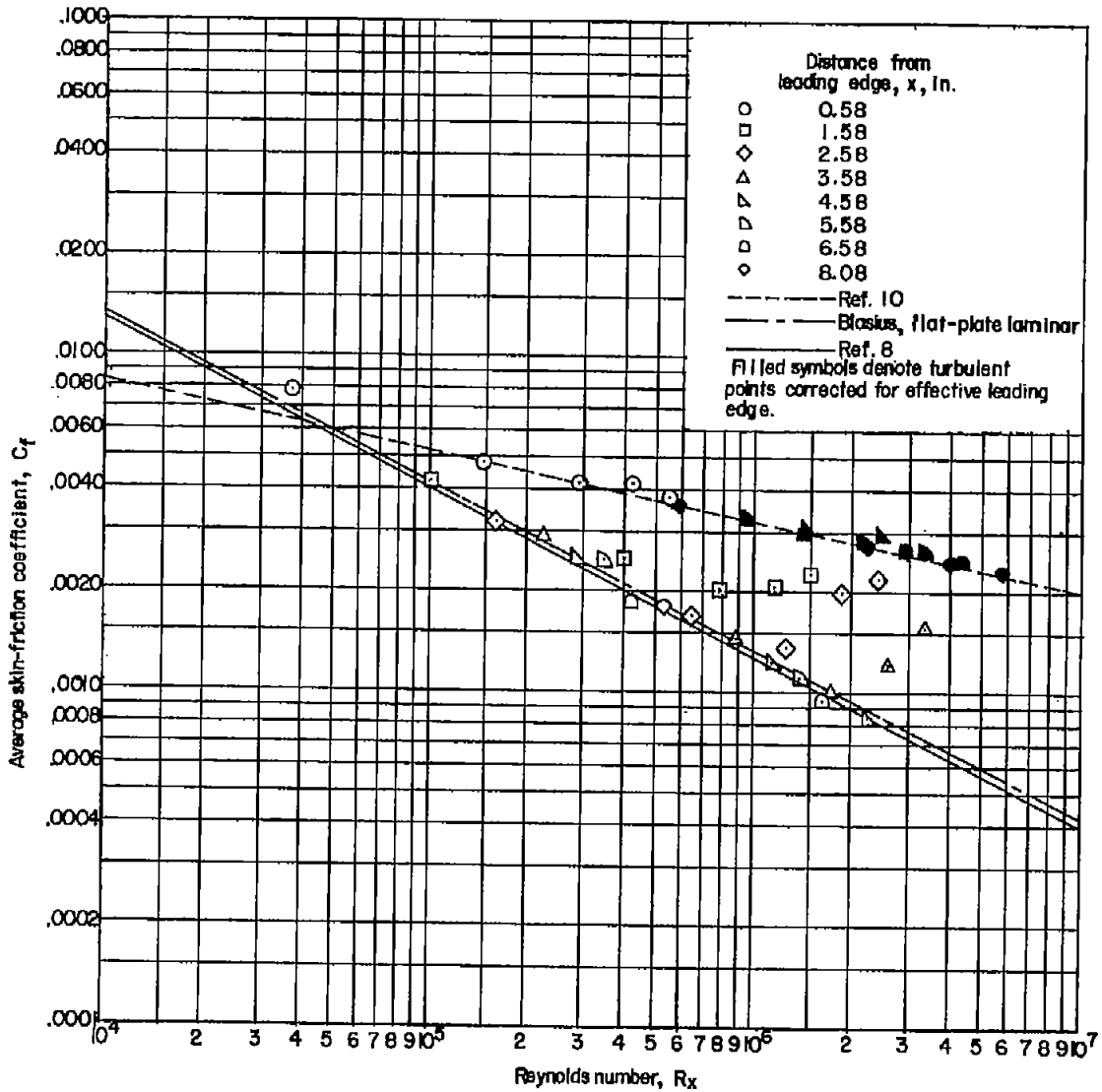

Figure 15.- Variation of average skin-friction coefficient with R_x.

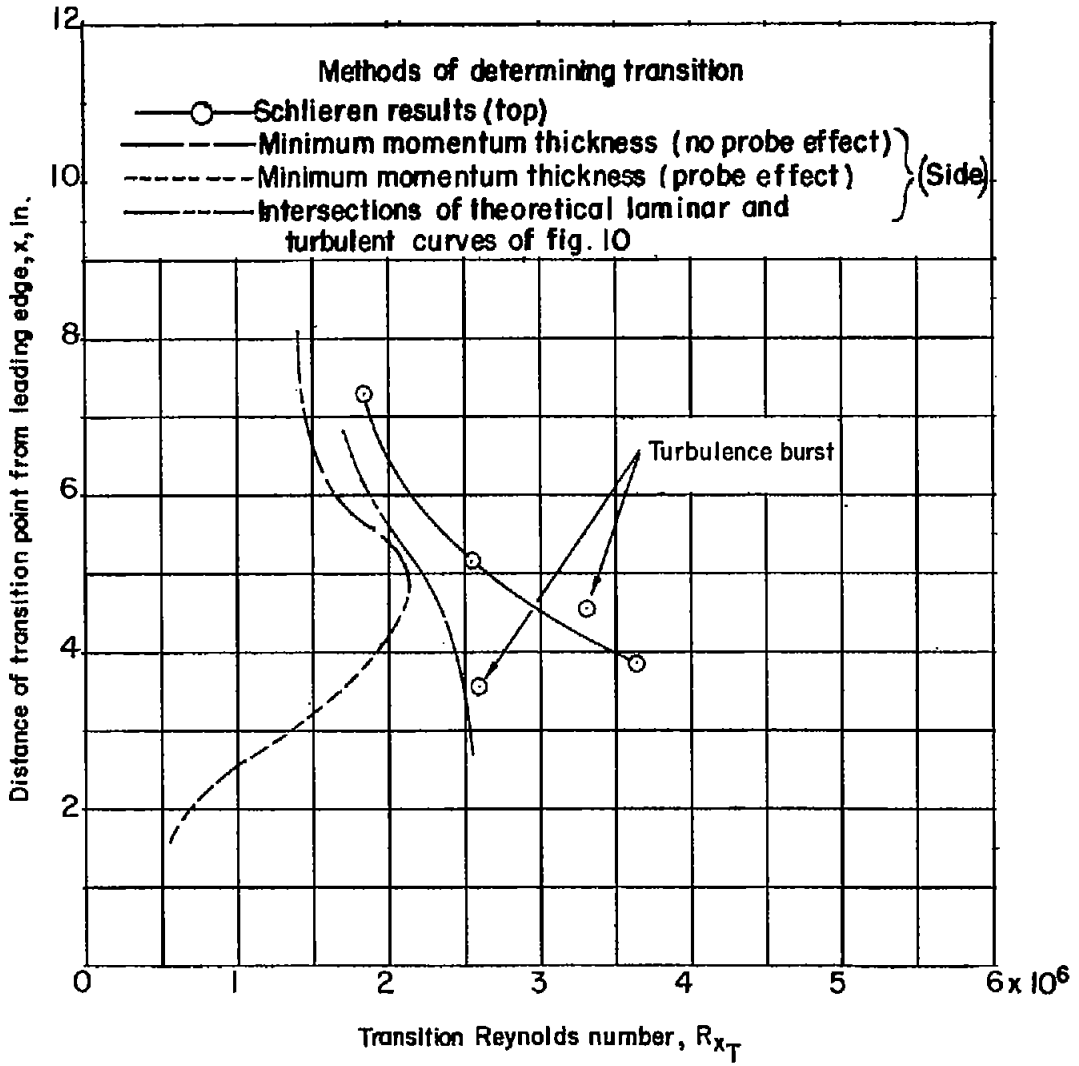

Figure 16.- Variation of transition location with transition Reynolds number.

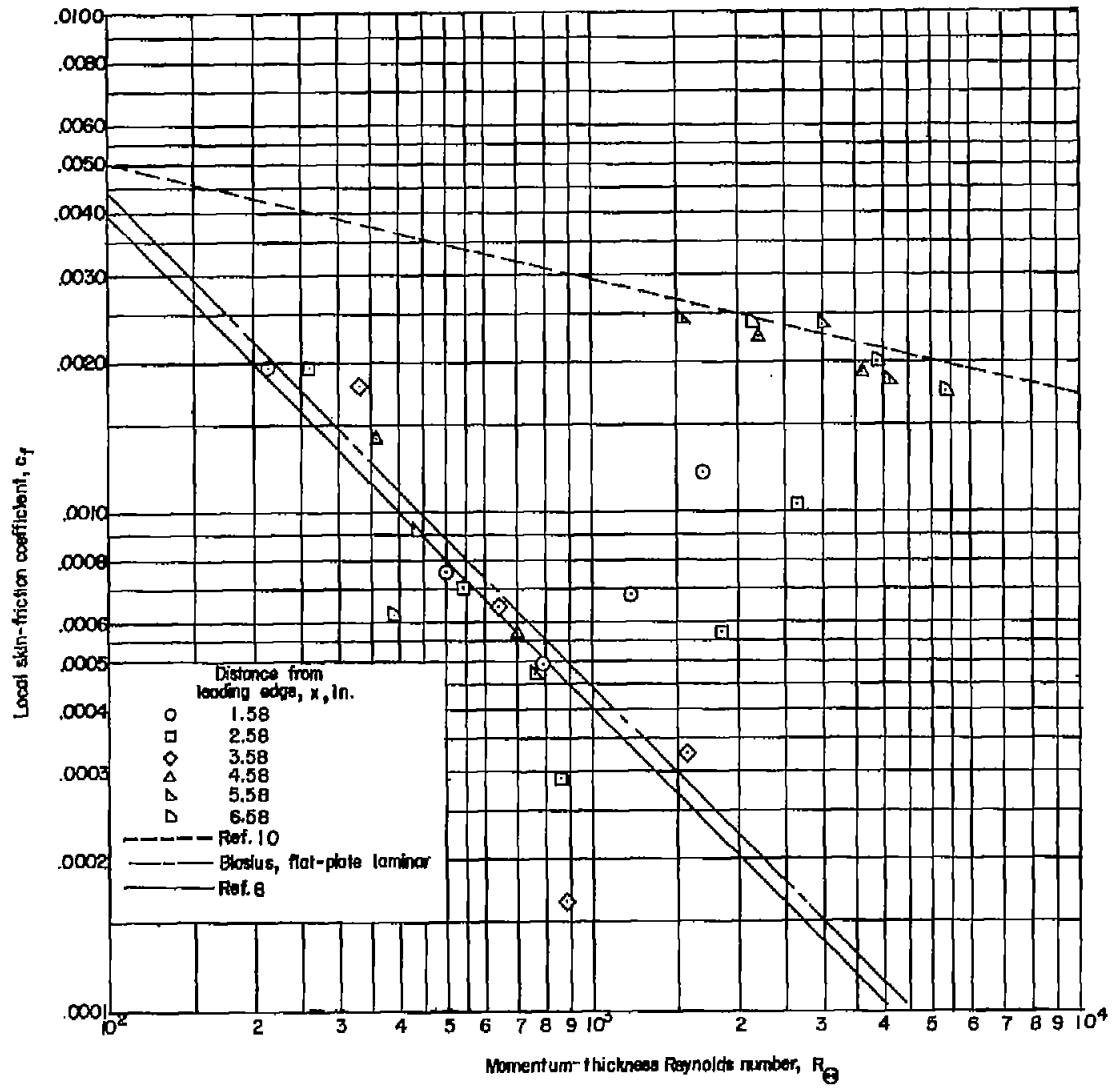

Figure 17.- Variation of local skin-friction coefficient with R_θ.

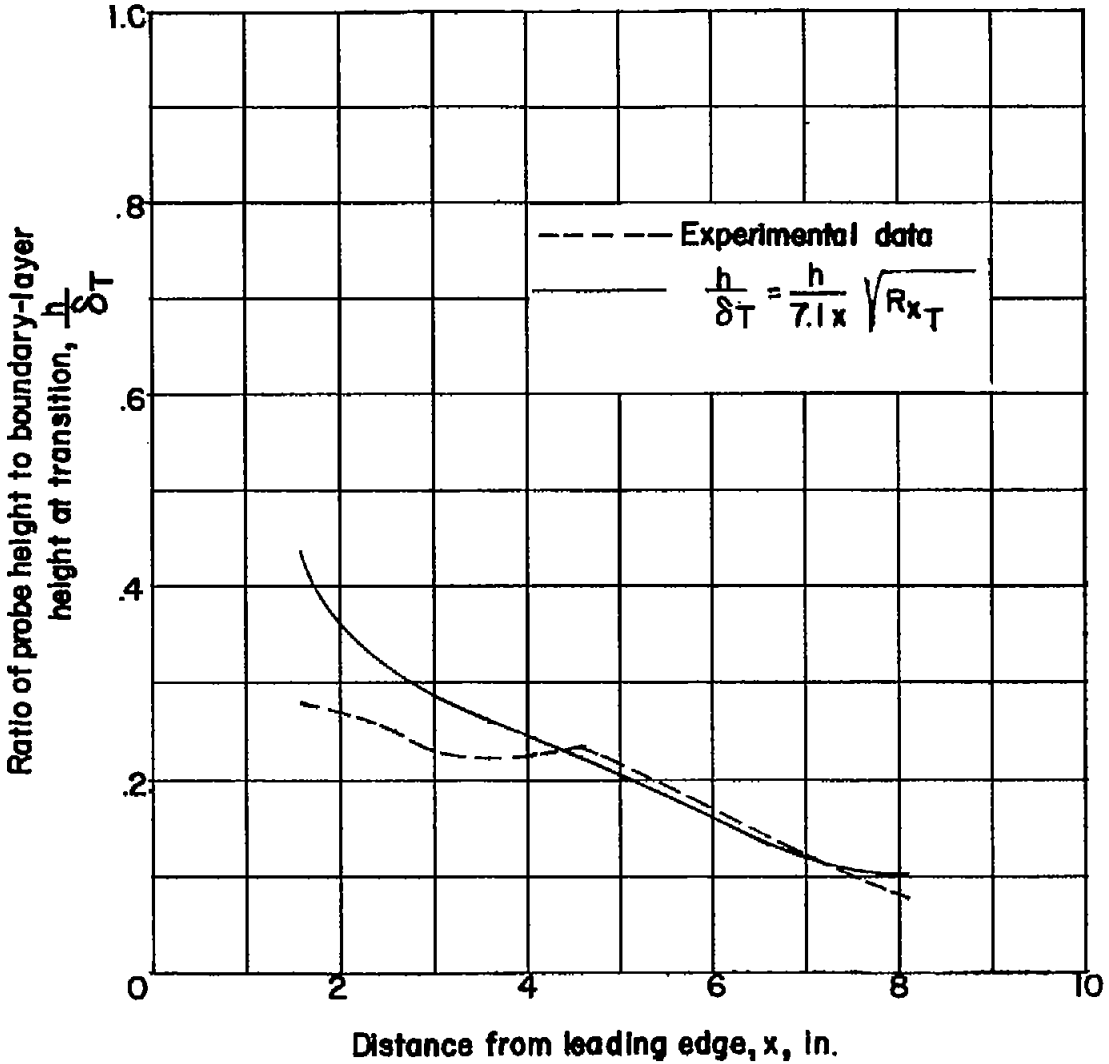

Figure 18.- Variation of h/δ_T with distance from leading edge of model.

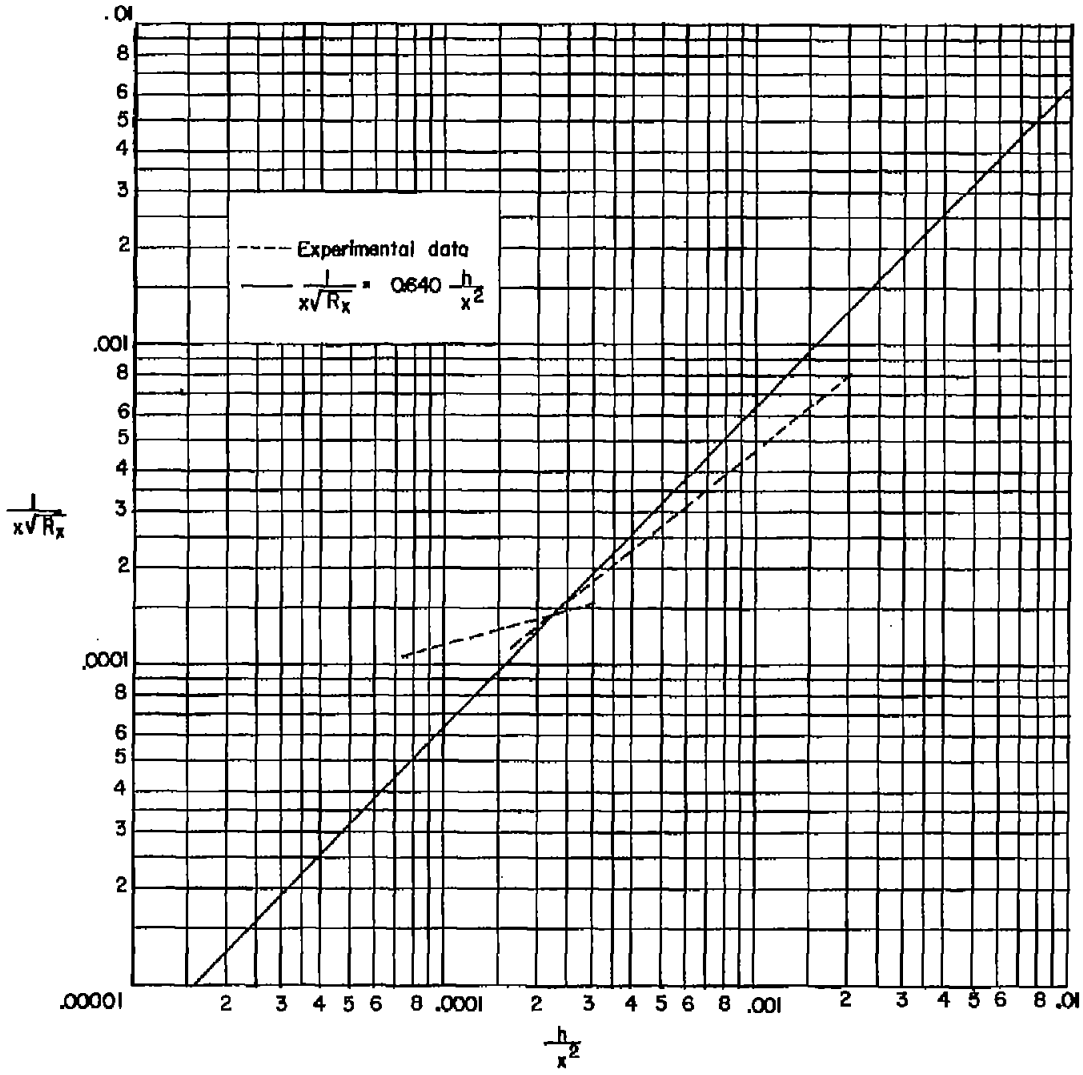

Figure 19.- Variation of $1/x\sqrt{R_x}$ as a function of h/x^2.

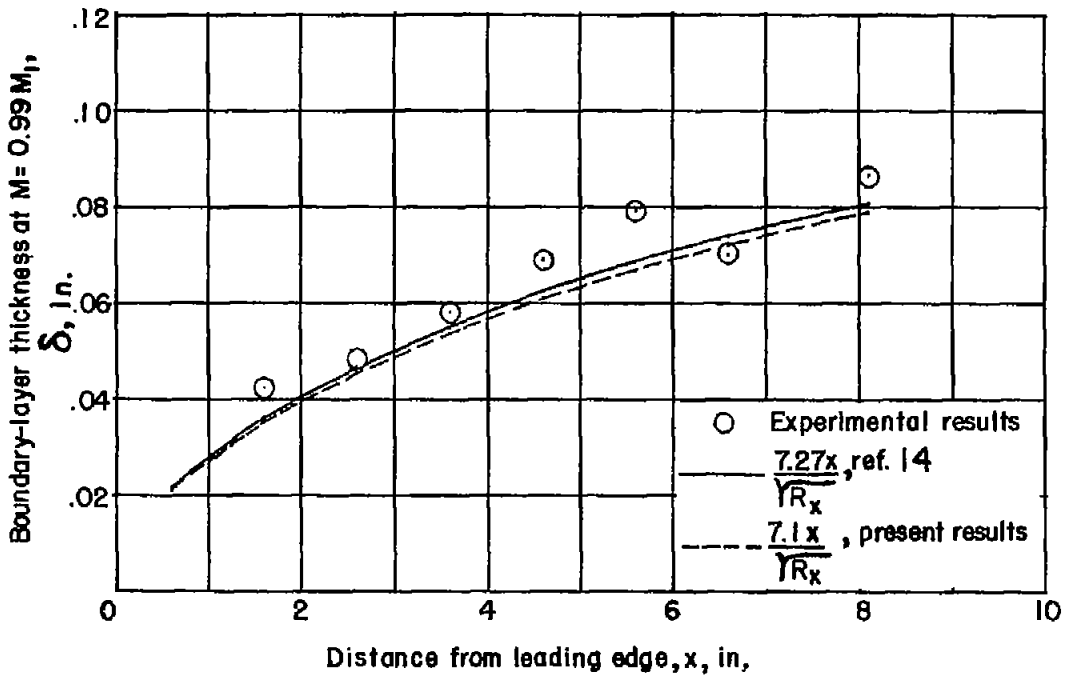

Figure 20.- Variation of laminar-boundary-layer thickness along the model at p_o = 7 in. Hg abs.